



HAL
open science

Structural and Magnetic Characterization of $\text{La}_{1+x}\text{Sr}_{1-x}\text{Co}_{0.5}\text{M}_{0.5}\text{O}_{4\pm\delta}$ (M=Cr, Mn)

Hany El Shinawi, Colin Greaves

► **To cite this version:**

Hany El Shinawi, Colin Greaves. Structural and Magnetic Characterization of $\text{La}_{1+x}\text{Sr}_{1-x}\text{Co}_{0.5}\text{M}_{0.5}\text{O}_{4\pm\delta}$ (M=Cr, Mn). *Journal of Inorganic and General Chemistry / Zeitschrift für anorganische und allgemeine Chemie*, 2009, 635 (12), pp.1856. 10.1002/zaac.200900202 . hal-00508909

HAL Id: hal-00508909

<https://hal.science/hal-00508909>

Submitted on 7 Aug 2010

HAL is a multi-disciplinary open access archive for the deposit and dissemination of scientific research documents, whether they are published or not. The documents may come from teaching and research institutions in France or abroad, or from public or private research centers.

L'archive ouverte pluridisciplinaire **HAL**, est destinée au dépôt et à la diffusion de documents scientifiques de niveau recherche, publiés ou non, émanant des établissements d'enseignement et de recherche français ou étrangers, des laboratoires publics ou privés.



Structural and Magnetic Characterization of $\text{La}_{1+x}\text{Sr}_{1-x}\text{Co}_{0.5}\text{M}_{0.5}\text{O}_{4\pm\delta}$ (M=Cr, Mn)

| | |
|-------------------------------|--|
| Journal: | <i>Zeitschrift für Anorganische und Allgemeine Chemie</i> |
| Manuscript ID: | zaac.200900202.R1 |
| Wiley - Manuscript type: | Article |
| Date Submitted by the Author: | 13-Jun-2009 |
| Complete List of Authors: | El Shinawi, Hany; University of Birmingham, School of Chemistry Greaves, Colin; University of Birmingham, School of Chemistry |
| Keywords: | Magnetic properties, Nonstoichiometric, Neutron diffraction, Layered compounds, Solid state reactions |
| | |



1
2
3 **Structural and Magnetic Characterization of $\text{La}_{1+x}\text{Sr}_{1-x}\text{Co}_{0.5}\text{M}_{0.5}\text{O}_{4\pm\delta}$**
4 **(M=Cr, Mn)**
5
6
7

8
9 **Hany El Shinawi and Colin Greaves***

10
11 *School of Chemistry, University of Birmingham, Birmingham B15 2TT, UK*
12
13

14
15
16
17 **Submitted to:**

18
19 Z Anorg Allg Chem
20
21
22
23
24
25

26
27 **Correspondence to:**

28
29 Prof C Greaves
30 School of Chemistry
31 University of Birmingham
32 Birmingham B15 2TT
33 UK
34

35
36
37 Email: c.greaves@bham.ac.uk
38
39
40
41
42
43
44
45
46
47
48
49
50
51
52
53
54
55
56
57
58
59
60

Abstract

The K_2NiF_4 phases $La_{1+x}Sr_{1-x}Co_{0.5}Cr_{0.5}O_{4\pm\delta}$ ($x=0, 0.15$) and $La_{1+x}Sr_{1-x}Co_{0.5}Mn_{0.5}O_{4\pm\delta}$ ($x=0, 0.2$) have been synthesised and examined by X-ray powder diffraction, thermal analysis, neutron powder diffraction and magnetic susceptibility measurements. Mn^{3+}/Co^{3+} and Cr^{3+}/Co^{3+} states predominate in the oxidised forms. Structural stability and crystal symmetry are retained under reducing conditions which cause reduction of Co^{3+} into Co^{2+} and the creation of oxide ion vacancies within the equatorial planes of the K_2NiF_4 structure. Excess oxygen in $La_{1.2}Sr_{0.8}Co_{0.5}Mn_{0.5}O_{4.1}$ is accommodated in the ideal interstitial positions (0, 0.5, 0.25) of the tetragonal structure. these materials depending upon the atmosphere applied. No long-range magnetic order has been observed because of competing AFM and FM interactions in these B-site disordered materials.

Keywords

Magnetic properties

Nonstoichiometric

Neutron diffraction

Layered compounds

Solid state reactions

Introduction

There are very few reports of perovskite-type oxides containing Co^{2+} in their B-sites. These phases are often prepared under oxygen-free or reducing conditions due to their susceptibility to oxidation by atmospheric air. Apart from La_2CoO_4 , the presence of Co^{2+} in perovskite-type oxides is often linked to oxide ion vacancies; $\text{La}_2\text{Co}_2\text{O}_5$, $\text{La}_4\text{Co}_3\text{O}_9$ and $\text{LaSrCoO}_{3.5+x}$ [1-3] are examples of such materials where oxide ion vacancies are either ordered or disordered. Octahedral, tetrahedral, pyramidal and even planar coordinations were assigned to Co in these materials, which indicate the flexibility of Co ions to accommodate a wide range of environments. These phases, however, are unstable in air and also have a limited stability under reducing conditions. On the other hand, stoichiometric K_2NiF_4 phases containing Co^{2+} or $\text{Co}^{2+}/\text{Co}^{3+}$ mixtures may be converted to oxygen hyperstoichiometric phases via oxidation of some Co^{2+} to Co^{3+} . This effect has been observed in $\text{La}_2\text{Co}(\text{M})\text{O}_{4+\delta}$ phases [4-6] where the excess oxygen is incorporated into the rock-salt region of the structure as interstitial defects. Oxygen hyperstoichiometry has also been suggested for strontium doped phases $(\text{La,Sr})\text{Co}^{\text{II,III}}\text{O}_4$ [7,8], but these materials have not been fully characterized.

This study aimed to utilize the variety of oxidation states and coordination flexibility of cobalt in layered perovskites to achieve oxygen nonstoichiometry (and mixed valency) that is stable in different oxygen partial pressure and temperature environments. Such materials may be of great interest in applications such as electrodes in solid oxide fuel cells and oxygen separation membranes. It has been found that La-Sr-Co-Fe-O K_2NiF_4 phases [9] containing either Co^{3+} or $\text{Co}^{2+}/\text{Co}^{3+}$ are able to withstand reducing conditions (10% H_2/N_2) up to 1000°C via reduction of Co^{3+} into Co^{2+} and formation of highly distorted MO_x polyhedra; however, the stoichiometric material containing $\text{Co}^{2+}/\text{Co}^{3+}$ ($\text{La}_{1.2}\text{Sr}_{0.8}\text{Co}_{0.5}\text{Fe}_{0.5}\text{O}_4$) showed no tendency toward oxygen hyperstoichiometry resulting from oxidation of Co^{2+} to Co^{3+} [9]. Two new materials of this type are reported here: $\text{La}_{1+x}\text{Sr}_{1-x}\text{Co}_{0.5}\text{Mn}_{0.5}\text{O}_{4\pm\delta}$ ($x=0, 0.2$) and $\text{La}_{1+x}\text{Sr}_{1-x}\text{Co}_{0.5}\text{Cr}_{0.5}\text{O}_{4\pm\delta}$ ($x=0, 0.15$). These materials exhibit a high degree of structural stability either in air or under reducing conditions at elevated temperatures, along with a range of oxygen nonstoichiometry including

1
2 hyperstoichiometry. We have also studied the two-dimensional M-M magnetic exchange
3
4 interactions in these phases.
5
6
7
8

9 10 Experimental

11 The materials $\text{La}_{1+x}\text{Sr}_{1-x}\text{Co}_{0.5}\text{Cr}_{0.5}\text{O}_{4\pm\delta}$ ($x = 0, 0.15$) and $\text{La}_{1+x}\text{Sr}_{1-x}\text{Co}_{0.5}\text{Mn}_{0.5}\text{O}_{4\pm\delta}$ ($x=0, 0.2$)
12 were synthesized by solid state reactions using high purity SrCO_3 , La_2O_3 , Co_3O_4 , Mn_2O_3 and Cr_2O_3
13 as the starting materials (all previously dried at 800°C in air for 12h in order to remove residual
14 water, hydroxide or carbonate). In order to obtain pure K_2NiF_4 phases, we used a two-step
15 procedure: stoichiometric amounts of starting materials were intimately mixed, pressed into pellets
16 and calcined at 1350°C for 30h under a N_2 atmosphere (as-prepared materials). The samples were
17 then ground and subsequently heated in air (at 750°C for 12h) or flowing 10% H_2/N_2 gas (at 750°C
18 for 12h) in order to prepare the “oxidized” and the “reduced” samples, respectively. All syntheses
19 involved standard furnace cooling regimes.
20
21
22
23
24
25
26
27
28
29
30
31
32

33 X-ray powder diffraction (XRD) data were collected using a Siemens D5000 diffractometer
34 in transmission mode, employing $\text{CuK}\alpha_1$ radiation from a germanium monochromator. Neutron
35 powder diffraction (NPD) data were collected at room temperature and 4 K on the D2B
36 diffractometer at the ILL, Grenoble, using a wavelength of 1.594 \AA and the HRPT diffractometer at
37 the SINQ, PSI, using a wavelength of 1.494 \AA . Rietveld refinement was performed on the powder
38 diffraction data using the GSAS suite of programs [10] employing a pseudo-Voigt peak shape. All
39 refinements required the use of correction for preferred orientation along [001] direction.
40 Thermogravimetric measurements were performed using a Rheometric Scientific STA 1500 thermal
41 analyzer. Measurements to analyze the reduction behaviour of the oxidized materials were
42 performed on ~ 30 mg samples heated at $10^\circ\text{C min}^{-1}$ in 10% H_2/N_2 . Magnetic susceptibility data
43 were collected using a Quantum Design PPMS magnetometer in the temperature range 5-300 K.
44 Zero-field-cooled (ZFC) and field-cooled (FC) data were collected on warming using an applied
45 field of 0.3 T.
46
47
48
49
50
51
52
53
54
55
56
57
58
59
60

Results

Structural Characterization

The phase purity and crystal structures of all the samples were examined by XRD. The data indicated that all materials are single-phase with no evidence of impurities or starting materials. XRD patterns were readily indexed on a body-centred tetragonal unit cell, consistent with a structure related to that of K_2NiF_4 (Figure 1). Structural refinements based on XRD data showed that the materials crystallize in the $I4/mmm$ space group; no evidence of peak splitting or systematic broadening, which may indicate a lowering of cell symmetry due to reduction, was observed. However, as expected from X-ray diffraction, the refinements were insensitive to oxygen nonstoichiometry in the reduced materials and the oxide ion sites could be fixed at full occupancy. A summary of the refined unit cell parameters for different samples is given in Table 1.

NPD data collected at room temperature were used to probe more reliably the oxygen content and defect structures of these materials. Refinement results from the data collected from the reduced materials at room temperature are given in Table 2. Unit cell sizes determined from XRD and NPD data (Tables 1 and 2) differ slightly, as is normal, because of the calibration errors inherent in NPD sources. The estimated standard deviations are from the statistics of the refinements and do not include these systematic errors. Profiles and difference patterns from the Rietveld analysis are shown in Figure 2. The oxygen contents are based on formal oxidation states of Co(II), Mn(III) and Cr(III), which are in excellent agreement with refined data (*vide infra*). Some selected bond lengths are given in Table 3. Refinements were performed adopting the ideal $I4/mmm$ space group; the use of lower symmetry tetragonal and orthorhombic space groups were unsuccessful and confirmed the absence of cation or defect order. It is important to note that the scattering length contrast is such that Co/Mn and Co/Cr ordering would have been easily detectable in these experiments [11]; such B-site cation order has previously been observed in Co-Mn perovskites [12].

Oxide ion vacancies in these materials are disordered and confined to the equatorial (Co/M)O₂ planes of the K₂NiF₄ structure (O1 in Figure 1). An attempt to fit a model in which oxide ion vacancies are distributed between axial and equatorial oxygen sites [13] proved unstable. An associated twisting of the (Co/M)O₆ octahedra around the z-axis is observed, which transforms the oxide ions at (0.5, 0, 0) to the split position (0.5, y, 0), similar to that observed in La_{1+x}Sr_{1-x}Co_{0.5}Fe_{0.5}O_{4-δ} [9]. Despite some correlation between thermal parameters and site occupancies, stable refinements were achieved without applying constraints.

Refinements gave the overall stoichiometries LaSrCo_{0.5}Cr_{0.5}O_{3.76}, La_{1.15}Sr_{0.85}Co_{0.5}Cr_{0.5}O_{3.82}, LaSrCo_{0.5}Mn_{0.5}O_{3.74} and La_{1.2}Sr_{0.8}Co_{0.5}Mn_{0.5}O_{3.84} for the reduced materials. Consideration of these results in conjunction with TG analysis data (Figure 3), in which the oxidized materials were reduced in flowing 10% H₂/N₂, provided the oxygen stoichiometries of the oxidized materials: LaSrCo_{0.5}Cr_{0.5}O₄, La_{1.15}Sr_{0.85}Co_{0.5}Cr_{0.5}O₄, LaSrCo_{0.5}Mn_{0.5}O₄ and La_{1.2}Sr_{0.8}Co_{0.5}Mn_{0.5}O_{4.1}. In order to confirm oxygen hyperstoichiometry in La_{1.2}Sr_{0.8}Co_{0.5}Mn_{0.5}O_{4.1}, NPD data were collected from this sample at room temperature. Profiles and structural data are given in Figure 4 and Table 4, respectively. Refinement supported the presence of interstitial oxygen and was consistent with the composition La_{1.2}Sr_{0.8}Co_{0.5}Mn_{0.5}O_{4.10(1)}. The excess oxygen occupies the ideal interstitial sites (0, 0.5, 0.25) of the tetragonal structure (O3 in Figure 1). An associated displacement of the apical oxide ions, related to that of Jorgensen's interstitial defect model [14], moves apical oxygen atoms from their ideal position at (0, 0, z) to the split position (0, y, z). Incorporation of excess interstitial oxygen in the K₂NiF₄ structure with retention of tetragonal symmetry has been observed in La_{1.2}Sr_{0.8}MnO_{4.27} [15]. No evidence of magnetic order was observed in the low temperature NPD data of any sample.

Magnetic Susceptibility:

Figure 5(a) shows the temperature dependence of the magnetic susceptibility of the chromium-containing samples. The oxidized materials are essentially paramagnetic, whereas a

1
2 distinct divergence between ZFC and FC susceptibilities is observed in the reduced materials, which
3 suggests spin glass behaviour. Plots of the reciprocal of the molar susceptibility against
4 temperature for the reduced samples (Figure 6(a)) suggest a non Curie-Weiss behaviour in the given
5 temperature range. However, the plots display an increase in gradient on cooling which is expected
6 for spin glasses with antiferromagnetic (AFM) interactions [16] or moments which are not
7 temperature independent, as expected for octahedral Co^{2+} . Application of the Curie-Weiss law at
8 the extreme parts of the plots provides negative θ values, which confirms predominantly AFM
9 interactions. Above 200 K, the θ values are -179.4 and -182.2 for $\text{LaSrCo}_{0.5}\text{Cr}_{0.5}\text{O}_{3.75}$ and
10 $\text{La}_{1.15}\text{Sr}_{0.85}\text{Co}_{0.5}\text{Cr}_{0.5}\text{O}_{3.825}$ respectively, and the effective moment for both is $3.84 \mu_{\text{B}}$ per formula
11 unit. The reciprocal susceptibility plots of the oxidized materials also indicate AFM exchange
12 interactions (see Figure 6(a)). Above 200 K, the θ values are -245.5 and -69.2 and the effective
13 moments are $3.88 \mu_{\text{B}}$ and $3.80 \mu_{\text{B}}$, for $\text{LaSrCo}_{0.5}\text{Cr}_{0.5}\text{O}_4$ and $\text{La}_{1.15}\text{Sr}_{0.85}\text{Co}_{0.5}\text{Cr}_{0.5}\text{O}_4$ respectively.
14 Variation of magnetic susceptibility with temperature for manganese-containing samples is shown
15 in Figure 5(b). The oxidized materials also show higher magnetization than the reduced ones. The
16 divergence between ZFC and FC susceptibilities is again suggestive of spin-glass behaviour. The
17 magnetic susceptibility of $\text{La}_{1.2}\text{Sr}_{0.8}\text{Co}_{0.5}\text{Mn}_{0.5}\text{O}_{3.85}$ shows a broad maximum at about 70 K, which is
18 an indication of AFM ordering in this 2D system. However, no evidence of magnetic order has been
19 found in the low temperature NPD data of this sample. A plot of the reciprocal of the molar
20 susceptibility against temperature for $\text{LaSrCo}_{0.5}\text{Mn}_{0.5}\text{O}_{3.75}$ shows departure from Curie-Weiss
21 behaviour. Again the plot displays decreasing effective moments with negative θ values on cooling
22 which is expected for spin glasses with AFM interactions (Figure 6(b)). On the other hand, the
23 reciprocal susceptibility plots of the oxidized materials indicate that these materials exhibit
24 exchange interactions which are predominantly ferromagnetic (FM) with positive θ values and an
25 increasing effective moment as the temperature decreases [16] (see Figure 6(b)).
26
27
28
29
30
31
32
33
34
35
36
37
38
39
40
41
42
43
44
45
46
47
48
49
50
51
52
53
54
55
56
57
58
59
60

Discussion

Oxygen stoichiometries based on refined NPD data and TG analysis of chromium-containing samples are very close to the theoretical values corresponding to $\text{Co}^{2+}/\text{Cr}^{3+}$ in the reduced materials and $\text{Co}^{3+}/\text{Cr}^{3+}$ in the oxidized materials, i.e. $\text{LaSrCo}_{0.5}\text{Cr}_{0.5}\text{O}_4$, $\text{LaSrCo}_{0.5}\text{Cr}_{0.5}\text{O}_{3.75}$, $\text{La}_{1.15}\text{Sr}_{0.8}\text{Co}_{0.5}\text{Cr}_{0.5}\text{O}_4$ and $\text{La}_{1.15}\text{Sr}_{0.85}\text{Co}_{0.5}\text{Cr}_{0.5}\text{O}_{3.825}$. These nominal stoichiometries are therefore adopted. The reduced materials are spin-glass antiferromagnets. This behaviour can be attributed to competing AFM and FM interactions between high-spin Co^{2+} and Cr^{3+} ions; according to Goodenough-Kanamori rules for superexchange interactions [17,18], a disordered Co/Cr distribution would result in competing FM (Co–Cr) and AFM (Co–Co and Cr–Cr) interactions. The effective moments for $\text{LaSrCo}_{0.5}\text{Cr}_{0.5}\text{O}_{3.75}$ and $\text{La}_{1.15}\text{Sr}_{0.85}\text{Co}_{0.5}\text{Cr}_{0.5}\text{O}_{3.85}$ near room temperature (both $3.84 \mu_B$) are consistent with high-spin Co^{2+} and Cr^{3+} ions ($3.87 \mu_B$), although a higher moment may be anticipated because of the orbital contribution to the magnetic moment expected for high-spin Co^{2+} .

The magnetic behaviour of the oxidized materials can be attributed to weak exchange consistent with Co^{3+} ions being in the low-spin state. The effective moments $2.88 \mu_B$ and $2.80 \mu_B$ for $\text{LaSrCo}_{0.5}\text{Cr}_{0.5}\text{O}_4$ and $\text{La}_{1.15}\text{Sr}_{0.8}\text{Co}_{0.5}\text{Cr}_{0.5}\text{O}_4$ are relatively close to the spin-only values based on high-spin $\text{Cr}^{3+}/\text{Co}^{2+}$ and low-spin Co^{3+} ions. Spin-only moments which are predicted for $\text{LaSrCo}^{\text{III}}_{0.5}\text{Cr}_{0.5}\text{O}_4$ and $\text{La}_{1.15}\text{Sr}_{0.8}\text{Co}^{\text{II/III}}_{0.5}\text{Cr}_{0.5}\text{O}_4$ are $2.74 \mu_B$ and $3.12 \mu_B$, respectively. Disappearance of the spin glass behaviour in these oxidised materials is supportive of a low spin state of Co^{3+} ; presence of Co^{3+} in the high-spin or intermediate-spin states would produce a ferromagnetic component of interactions [$\text{Co}^{3+} (t_{eg}^4 e_g^2)$ - $\text{Cr}^{3+} (t_{2g}^3 e_g^0)$]/ $\text{Co}^{3+} (t_{eg}^5 e_g^1)$ - $\text{Cr}^{3+} (t_{2g}^3 e_g^0)$] which may result in a spin glass state at low temperatures.

The manganese-containing phases have compositions $\text{LaSrCo}_{0.5}\text{Mn}_{0.5}\text{O}_4$ and $\text{La}_{1.2}\text{Sr}_{0.8}\text{Co}_{0.5}\text{Mn}_{0.5}\text{O}_{4.1}$ (oxidized materials) with reduced forms $\text{LaSrCo}_{0.5}\text{Mn}_{0.5}\text{O}_{3.75}$ and $\text{La}_{1.2}\text{Sr}_{0.8}\text{Co}_{0.5}\text{Mn}_{0.5}\text{O}_{3.85}$. Adopting these stoichiometries for the reduced materials suggests the oxidation states $\text{Co}^{2+}/\text{Mn}^{3+}$ or $\text{Co}^{3+}/\text{Mn}^{2+}$ for Co and Mn in these materials. Based on arguments given by Karen et al [19], and consistency of Co behaviour in similar systems

(La_{1+x}Sr_{1-x}Co_{0.5}Mn_{0.5}O_{4-δ} M=Fe [9] and Cr), formation of Co²⁺ (rather than Mn²⁺) under reduction to neutralize oxygen deficiency in these materials is favoured. The presence of the oxidation states Co²⁺ and Mn³⁺ in the reduced materials rationalizes the spin glass state and absence of long-range AFM order in La_{1.2}Sr_{0.8}Co_{0.5}Mn_{0.5}O_{3.85} since we predict competing AFM and FM interactions, where the Co²⁺-Co²⁺ interactions are AFM, Mn³⁺-Mn³⁺ and Co²⁺-Mn³⁺ interactions are FM/AFM [17,18].

NPD analysis showed no evidence of cation order in any of the studied materials which is consistent with the absence of Co²⁺/Mn⁴⁺ charge states in the oxidized materials; the ordered Co²⁺/Mn⁴⁺ state is also unexpected since it would produce long-range FM order [20] which is not observed in this study. This information suggests the Co³⁺/Mn³⁺ states to be present in LaSrCo_{0.5}Mn_{0.5}O₄ and La_{1.2}Sr_{0.8}Co_{0.5}Mn_{0.5}O_{4.1}. The stoichiometric phase La_{1.2}Sr_{0.8}Co_{0.5}Mn_{0.5}O₄ has not been characterized in this study but it would be expected to contain a mixture of Mn³⁺, Co³⁺ and Co²⁺ ions. The excess oxygen content in La_{1.2}Sr_{0.8}Co_{0.5}Mn_{0.5}O_{4.1} suggests instability linked to the facile oxidation of Co²⁺ into Co³⁺. However, the absence of oxygen hyperstoichiometry in La_{1.2}Sr_{0.8}Co_{0.5}Fe_{0.5}O₄ [9] and La_{1.15}Sr_{0.85}Co_{0.5}Cr_{0.5}O₄ under similar oxidation conditions suggests that other factors are also involved.

The predominance of Co³⁺/Mn³⁺ oxidation states in the oxidized materials means that a low-spin state of Co³⁺ can account for the different magnetic behaviours of the oxidized and reduced materials. The enhanced FM exchange of the oxidized materials can be attributed to FM interaction between low-spin Co³⁺ and high-spin Mn³⁺; the absence of long range effect and hence the spin glass behaviour at low temperature are due to competition with the AFM nature of the Mn³⁺-Mn³⁺ interactions. The possibility of low concentrations of Co²⁺ and Mn⁴⁺ further complicates the magnetic interactions.

The TG data indicate that the studied materials withstand reducing conditions (10% H₂/N₂) up to 1000°C with retention of structural stability (as tested by XRD). Excessive reduction in the case of the Co-Mn samples at T > 800°C (Figure 3-b) indicates formation of some Mn²⁺ under these

1
2 conditions, with a correspondingly higher degree of oxygen deficiency. The presence of large
3
4 oxygen nonstoichiometry along with the structural stability at high temperature in reducing
5
6 environments makes these materials an attractive system to be explored for use as oxygen
7
8 separation membranes.
9

10
11 Oxide ion vacancies in the reduced materials are located within the equatorial planes of the
12
13 K_2NiF_4 structure, which suggests formation of unusual MO_x coordination polyhedra similar to those
14
15 observed in $LaSrCoO_{3.5+x}$ [3]. Vacancies in these materials are formed via reduction of low-spin
16
17 Co^{3+} into high-spin Co^{2+} which indicates an associated expansion in the MO_x polyhedra. An
18
19 expansion in a and c parameters is therefore expected, but expansion of a in these materials is often
20
21 hindered by the coordination requirements of the A-type (La/Sr) ions (see Table 1). Under
22
23 reduction, a contraction in La/Sr coordination sphere (achieved in the xy plane, i.e. a) occurs due to
24
25 reduction of coordination number (< 9) [3,9]. This explains the twist of MO_x polyhedra around the
26
27 z -axis in the reduced materials, where a contraction in a is required without significant contraction
28
29 of the MO_x polyhedra. The effect of interstitial oxygen on the lattice parameters of these materials
30
31 can also be examined by considering the refined NPD data of $La_{1.2}Sr_{0.8}Co_{0.5}Mn_{0.5}O_{4.1}$ and
32
33 $La_{1.2}Sr_{0.8}Co_{0.5}Fe_{0.5}O_4$ [9] and their reduced forms. 3.0% contraction in c and 1.2% expansion in a in
34
35 case of $La_{1.2}Sr_{0.8}Co_{0.5}Mn_{0.5}O_{4.1}$, compared with 1.8% and 0.2% in case of $La_{1.2}Sr_{0.8}Co_{0.5}Fe_{0.5}O_4$,
36
37 occur due to insertion of oxygen in these materials (starting from $O_{3.85}$ phases). Extra contraction of
38
39 c and expansion of a in $La_{1.2}Sr_{0.8}Co_{0.5}Mn_{0.5}O_{4.1}$ are therefore attributed to the interstitial oxygen; the
40
41 increase of the effective charge of the transition metal ions (to compensate the excess oxygen) can
42
43 account for the c contraction, while the expansion of a can be attributed to an expansion in the
44
45 coordination sphere of A ions (La/Sr), achieved also in the xy plane, due to an increase in the
46
47 coordination number (> 9).
48
49
50
51
52
53
54
55

56
57 Tables 2 and 3 clearly show a stronger distortion effect in MO_6 polyhedra for the
58
59 manganese-containing samples; this effect is associated with a significant elongation parallel to the
60
61 z axis ($LaSrCo_{0.5}Cr_{0.5}O_{3.75}$: $a=3.83401(4)$ Å, $c=12.72734(25)$ Å, $M-O1=1.9220(3)$ and

1
2 M-O2=2.125(2); LaSrCo_{0.5}Mn_{0.5}O_{3.75}: $a= 3.80329(6)$ Å, $c=13.04087(24)$ Å, M-O1=1.9076(2) and
3
4 M-O2=2.2269(9)). This effect is expected for Mn³⁺ because of its susceptibility to Jahn Teller
5
6 distortions [21].
7
8
9

10 11 12 13 14 15 16 17 18 19 20 21 22 23 24 25 26 27 28 29 30 31 32 33 34 35 36 37 38 39 40 41 42 43 44 45 46 47 48 49 50 51 52 53 54 55 56 57 58 59 60

Conclusions

La_{1+x}Sr_{1-x}Co_{0.5}Mn_{0.5}O_{4±δ} (x= 0, 0.2) and La_{1+x}Sr_{1-x}Co_{0.5}Cr_{0.5}O_{4±δ} (x=0, 0.15) are new members of mixed-cation K₂NiF₄ phases. The materials crystallize in the tetragonal *I4/mmm* space group and withstand reducing conditions (10% H₂/N₂ up to 1000°C) *via* reduction of Co³⁺ to Co²⁺ and formation of disordered oxide ion vacancies within the basal plane of the K₂NiF₄ structure. Under oxidizing conditions (air up to 1000°C), excess oxygen is introduced into the Sr-deficient sample containing Mn, forming La_{1.2}Sr_{0.8}Co_{0.5}Mn_{0.5}O_{4.1} with interstitial oxygen at (0, 0.5, 0.25) sites of the tetragonal structure. The reason for the inability of LaSrCo_{0.5}Mn_{0.5}O₄ and La_{1.15}Sr_{0.85}Co_{0.5}Cr_{0.5}O₄ to accommodate interstitial oxygen is not clear, but may relate to subtle redox effects of the B-site cations. Unlike the double perovskite La₂CoMnO₆ [12], the layered nature of La_{1+x}Sr_{1-x}Co_{0.5}Mn_{0.5}O_{4±δ} stabilizes the Co³⁺/Mn³⁺ state which is converted into the Co²⁺/Mn³⁺ state under reduction; the dominant exchange interactions change from FM to AFM under reduction which is consistent with a low-spin state of Co³⁺ in these materials. The absence of long range magnetic order in all phases can be attributed to competing AFM and FM interactions which are consistent with the B-site disorder and layered nature of these materials.

Acknowledgements

We thank the Egyptian Education Bureau (London) for financial support (H. El Shinawi). We are also grateful to E. Suard and V. Pomjakushin for assistance with the collection of NPD data.

References

- [1] O. H. Hansteen, H. Fjellvag, B. C. Hauback, *J. Solid State Chem.* **1998**, 141, 411.
- [2] O. H. Hansteen, H. Fjellvag, B. C. Hauback, *J. Mater Chem.* **1998**, 8, 2089.
- [3] M. A. Hayward, M. J. Rosseinsky, *Chem. Mater.* **2000**, 12, 2182.
- [4] R. Le Toquin, W. Paulus, A. Cousson, and G. Dhalenne, A. Revcolevschi, *Physica B: Condensed Matter* **2004**, 350, E269.
- [5] A. Lappas, K. Prassides, *J. Solid State Chem.* **1994**, 108, 59.
- [6] G. Amow, P. S. Whitfield, I. J. Davidson, R. P. Hammond, C. N. Munnings, S. J. Skinner, *Ceramics International* **2004**, 30, 1635.
- [7] V. V. Vashook, H. Ullmann, O. P. Olshevskaya, V. P. Kulik, V. E. Lukashevich, L. V. Kokhanovskij, *Solid State Ionics* **2000**, 138, 99.
- [8] M. James, A. Tedesco, D. Cassidy, M. Colella, P. J. Smythe, *J. Alloys Compd.* **2006**, 419, 201.
- [9] H. El Shinawi, C. Greaves, *J. Solid State Chem.* **2008**, 181, 2705.
- [10] A.C. Larson, R.B. Von Dreele, *General Structural Analysis System*, Los Alamos National Laboratory, Los Alamos, NM, 1994.
- [11] V. K. Sears, *Neutron News* **1992**, 3, 29.
- [12] C. L. Bull, D. Gleeson, K. S. Knight, *J. Phys.: Condens. Matter* **2003**, 15, 4927.
- [13] P.H. Labbe, M. Ledesert, V. Caignaert, B. Raveau, *J. Solid State Chem.* **1991**, 91, 362.
- [14] J. D. Jorgensen, B. Dabrowski, Shiyou Pei, D. R. Richards, D. G. Hinks, *Phys. Rev. B* **1989**, 40, 2187.
- [15] R. K. Li, C. Greaves, *J. Solid State Chem.* **2000**, 153, 34.
- [16] K.V. Rao, M. Fahnle, E. Figueroa, O. Beckman, L. Hedman, *Phys. Rev. B* **1983**, 27, 3104.

- 1
2 [17] J. B. Goodenough, *Magnetism and the Chemical Bond*, Interscience, New York,
3
4 1963.
5
6
7 [18] J. Kanamori, *J. Phys. Chem. Solids* **1959**, 10, 87.
8
9 [19] P. Karen, E. Suard, F. Fauth, P. M. Woodward, *Solid State Sciences* **2004**, 6, 1195.
10
11 [20] R. I. Dass, J. B. Goodenough. *Phys. Rev. B* **2003**, 67, 014401.
12
13 [21] P. Ganguly, C. N. R. Rao, *J. Solid State Chem.* **1984**, 53, 193.
14
15
16
17
18
19
20
21
22
23
24
25
26
27
28
29
30
31
32
33
34
35
36
37
38
39
40
41
42
43
44
45
46
47
48
49
50
51
52
53
54
55
56
57
58
59
60

Table 1 XRD refined parameters for different samples (ox: oxidized & red: reduced).

| Material | a (Å) | c (Å) |
|--|------------|------------|
| LaSrCo_{0.5}Cr_{0.5}O₄-ox | 3.83249(5) | 12.4876(2) |
| LaSrCo_{0.5}Cr_{0.5}O₄-red | 3.82042(5) | 12.6753(3) |
| La_{1.15}Sr_{0.85}Co_{0.5}Cr_{0.5}O₄-ox | 3.84393(5) | 12.4974(2) |
| La_{1.15}Sr_{0.85}Co_{0.5}Cr_{0.5}O₄-red | 3.83330(7) | 12.6431(4) |
| LaSrCo_{0.5}Mn_{0.5}O₄-ox | 3.81967(5) | 12.5446(2) |
| LaSrCo_{0.5}Mn_{0.5}O₄-red | 3.77952(8) | 12.9785(3) |
| La_{1.2}Sr_{0.8}Co_{0.5}Mn_{0.5}O₄-ox | 3.83313(9) | 12.5854(4) |
| La_{1.2}Sr_{0.8}Co_{0.5}Mn_{0.5}O₄-red | 3.79130(3) | 12.9624(2) |

Table 2 Structural results for the refinement of the NPD data collected from the reduced samples at room temperature.

| Atom | x | y | z | 100 x Uiso (Å ²) | Occupancy | Site Symmetry |
|--|-----|-----------|------------|------------------------------|-------------|---------------|
| LaSrCo_{0.5}Cr_{0.5}O_{3.75}, $a = 3.83401(4)$ Å; $c = 12.72734(25)$ Å wRp = 0.0468; Rp = 0.0362; $\chi^2 = 1.479$ | | | | | | |
| Co/Cr | 0 | 0 | 0 | 0.83(5) | 0.5/0.5 | 2a |
| La/Sr | 0 | 0 | 0.3582(1) | 1.14(2) | 0.5/0.5 | 4e |
| O1 | 0.5 | 0.036(1) | 0 | 1.07(6) | 0.439(2) | 8j |
| O2 | 0 | 0 | 0.1670(1) | 2.05(4) | 1 | 4e |
| La_{1.15}Sr_{0.85}Co_{0.5}Cr_{0.5}O_{3.825}, $a = 3.84641(6)$ Å; $c = 12.7013(5)$ Å wRp = 0.0355; Rp = 0.0267; $\chi^2 = 2.34$ | | | | | | |
| Co/Cr | 0 | 0 | 0 | 0.76(7) | 0.5/0.5 | 2a |
| La/Sr | 0 | 0 | 0.3589(1) | 1.12(3) | 0.575/0.425 | 4e |
| O1 | 0.5 | 0.036(1) | 0 | 0.87(8) | 0.454(3) | 8j |
| O2 | 0 | 0 | 0.1685(2) | 2.05(5) | 1 | 4e |
| LaSrCo_{0.5}Mn_{0.5}O_{3.75}, $a = 3.80329(6)$ Å; $c = 13.04087(24)$ Å wRp = 0.0239; Rp = 0.018; $\chi^2 = 2.511$ | | | | | | |
| Co/Mn | 0 | 0 | 0 | 0* | 0.5/0.5 | 2a |
| La/Sr | 0 | 0 | 0.35687(5) | 0.86(2) | 0.5/0.5 | 4e |
| O1 | 0.5 | 0.0397(6) | 0 | 0.83(5) | 0.436(2) | 8j |
| O2 | 0 | 0 | 0.17076(7) | 2.05(3) | 1 | 4e |
| La_{1.2}Sr_{0.8}Co_{0.5}Mn_{0.5}O_{3.85}, $a = 3.81188(8)$ Å; $c = 13.0423(3)$ Å wRp = 0.0357; Rp = 0.0281; $\chi^2 = 2.14$ | | | | | | |
| Co/Mn | 0 | 0 | 0 | 0* | 0.5/0.5 | 2a |
| La/Sr | 0 | 0 | 0.35772(5) | 0.49(2) | 0.6/0.4 | 4e |
| O1 | 0.5 | 0.0280(9) | 0 | 0.68(5) | 0.461(3) | 8j |
| O2 | 0 | 0 | 0.17346(8) | 1.53(3) | 1 | 4e |

* Slightly negative temperature factor constrained to zero.

1
2
3
4
5
6
7
8
9
10
11
12
13
14
15
16
17
18
19
20
21
22
23
24
25
26
27
28
29
30
31
32
33
34
35
36
37
38
39
40
41
42
43
44
45
46
47
48
49
50
51
52
53
54
55
56
57
58
59
60**Table 3 Selected bond lengths (Å) for the refined phases.**

| Bond | LaSrCo _{0.5} Cr _{0.5} O _{3.75} | La _{1.15} Sr _{0.85} Co _{0.5} Cr _{0.5} O _{3.825} | LaSrCo _{0.5} Mn _{0.5} O _{3.75} | La _{1.2} Sr _{0.8} Co _{0.5} Mn _{0.5} O _{3.85} |
|-----------|---|--|---|---|
| Co/M-O1* | 1.9220(3) | 1.9281(4) | 1.9076(2) | 1.9089(2) |
| Co/M-O2 | 2.125(2) | 2.140(2) | 2.2269(9) | 2.262(1) |
| La/Sr-O1* | 2.534(3) | 2.529(4) | 2.559(2) | 2.585(3) |
| | 2.736(3) | 2.731(4) | 2.774(2) | 2.738(3) |
| La/Sr-O2 | 2.434(2) | 2.418(3) | 2.427(1) | 2.403(1) |
| | 2.7299(2) | 2.7420(4) | 2.7134(2) | 2.7259(2) |

*Splitting of O1 sites gives twice the number of bonds compared with the ideal site

Table 4 Structural results for the refinement of the NPD data collected from La_{1.2}Sr_{0.8}Co_{0.5}Mn_{0.5}O_{4.1} at room temperature.

| La _{1.2} Sr _{0.8} Co _{0.5} Mn _{0.5} O _{4.1} , $a = 3.85865(8)$ Å; $c = 12.6523(3)$ Å; $wRp = 0.0307$; $Rp = 0.0241$; $\chi^2 = 2.761$ | | | | | | | | |
|--|-----|----------|------------|------------------------------|-----------|---------------|------------|-----------------|
| Atom | x | y | z | 100 x Uiso (Å ²) | Occupancy | Site Symmetry | Bond | Bond Length (Å) |
| | | | | | | | Co/Mn-O1 | 1.92933(4) |
| Co/Mn | 0 | 0 | 0 | 0* | 0.5/0.5 | 2a | Co/Mn-O2** | 2.117(1) |
| La/Sr | 0 | 0 | 0.35905(6) | 0.66(3) | 0.6/0.4 | 4e | La/Sr-O1 | 2.6273(5) |
| O1 | 0.5 | 0 | 0 | 0.92(3) | 1 | 4c | La/Sr-O2** | 2.431(2) |
| O2 | 0 | 0.028(3) | 0.1671(1) | 2.04(8) | 0.25 | 16n | | 2.673(7) |
| O3 | 0 | 0.5 | 0.25 | 1.1(6) | 0.048(4) | 4d | | 2.827(7) |
| | | | | | | | La/Sr-O3 | 2.3719(5) |

*negative Uiso constrained to zero.

**Splitting of O2 sites gives 4 times the number of bonds compared with the ideal site.

Figure Captions

Figure 1. Crystal structure of $\text{La}_{1+x}\text{Sr}_{1-x}\text{Co}_{0.5}\text{M}_{0.5}\text{O}_{4\pm\delta}$ (M=Cr,Mn).

Figure 2. Observed, calculated and difference NPD profiles for data collected from the reduced samples at room temperature.

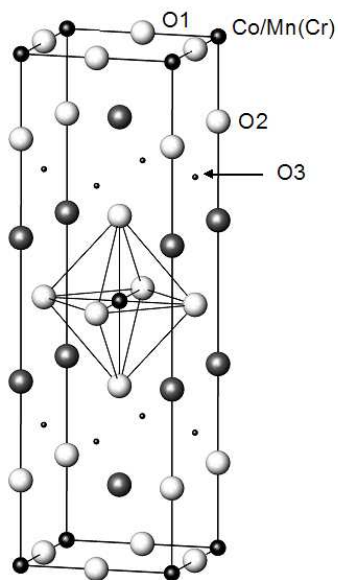
Figure 3. TG data for the reduction of oxidized materials using 10% H_2 in N_2 .

Figure 4. Observed, calculated and difference profiles for NPD data collected from $\text{La}_{1.2}\text{Sr}_{0.8}\text{Co}_{0.5}\text{Mn}_{0.5}\text{O}_{4.1}$ at room temperature.

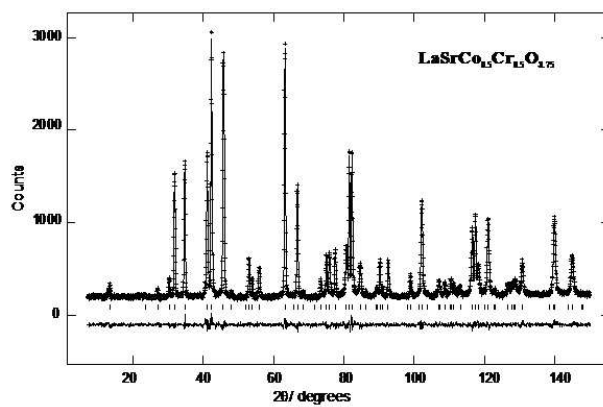
Figure 5. Variation of magnetic susceptibility (ZFC and FC) with temperature for (a) Cr-containing samples and (b) Mn-containing samples. Where FC and ZFC data deviate, the lower susceptibility corresponds with ZFC measurements.

Figure 6. Variation of the inverse magnetic susceptibilities (ZFC) with temperature.

1
2
3
4
5
6
7
8
9
10
11
12
13
14
15
16
17
18
19
20
21
22
23
24
25
26
27
28
29
30
31
32
33
34
35
36
37
38
39
40
41
42
43
44
45
46
47
48
49
50
51
52
53
54
55
56
57
58
59
60

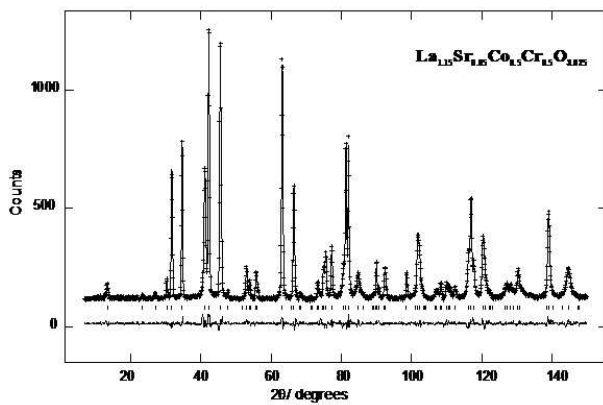


254x190mm (96 x 96 DPI)

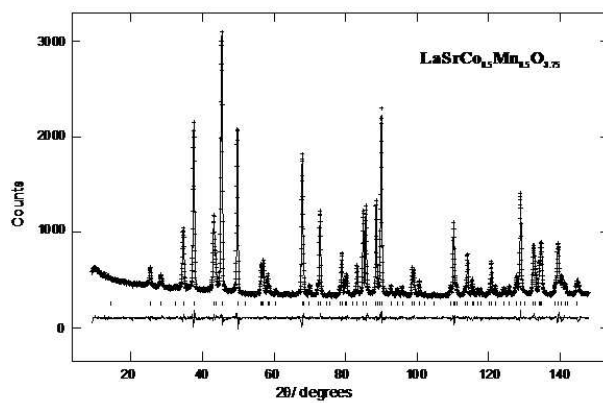


254x190mm (96 x 96 DPI)

1
2
3
4
5
6
7
8
9
10
11
12
13
14
15
16
17
18
19
20
21
22
23
24
25
26
27
28
29
30
31
32
33
34
35
36
37
38
39
40
41
42
43
44
45
46
47
48
49
50
51
52
53
54
55
56
57
58
59
60

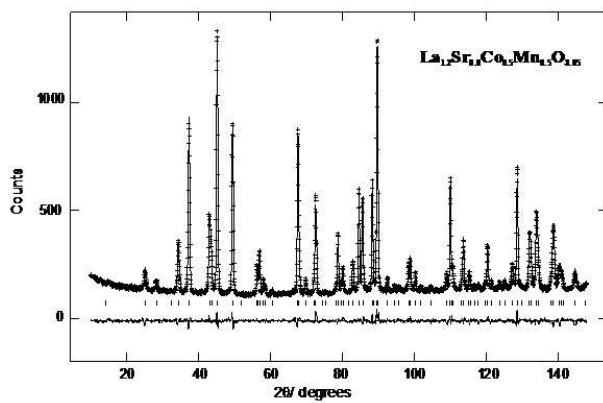


254x190mm (96 x 96 DPI)

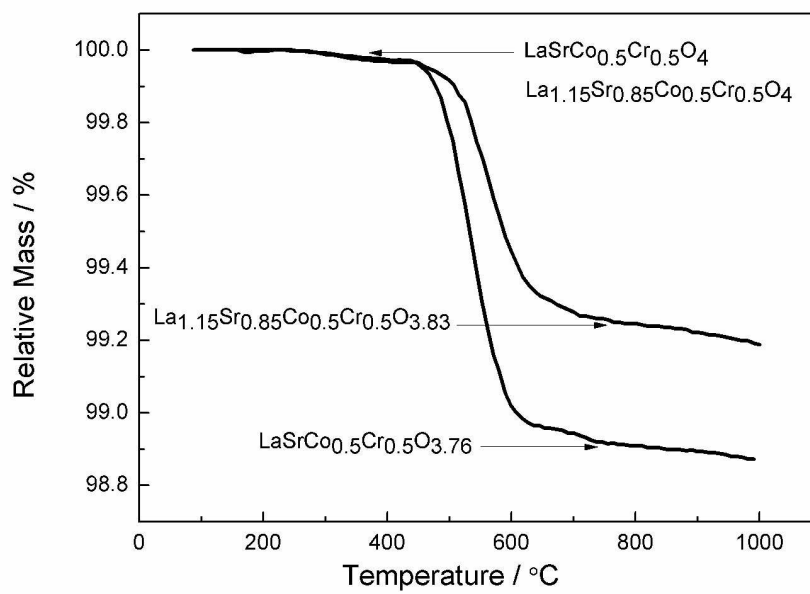


254x190mm (96 x 96 DPI)

1
2
3
4
5
6
7
8
9
10
11
12
13
14
15
16
17
18
19
20
21
22
23
24
25
26
27
28
29
30
31
32
33
34
35
36
37
38
39
40
41
42
43
44
45
46
47
48
49
50
51
52
53
54
55
56
57
58
59
60

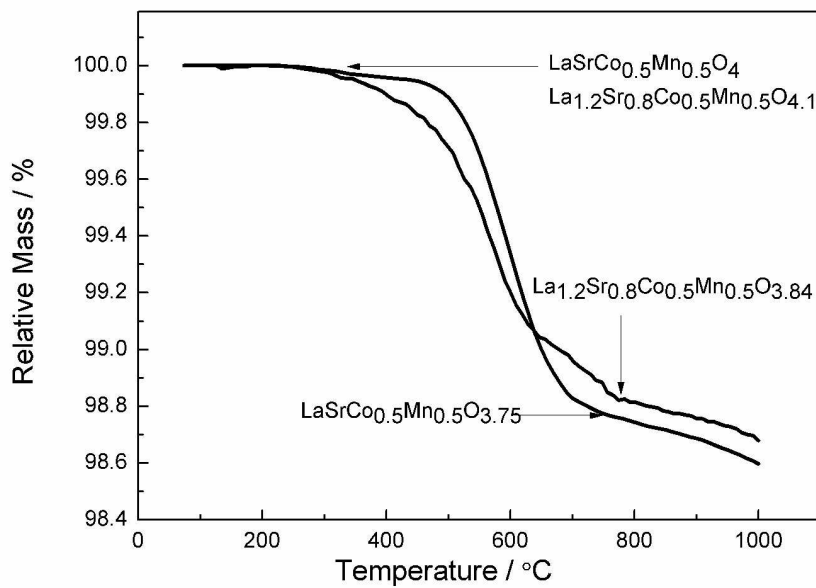


254x190mm (96 x 96 DPI)

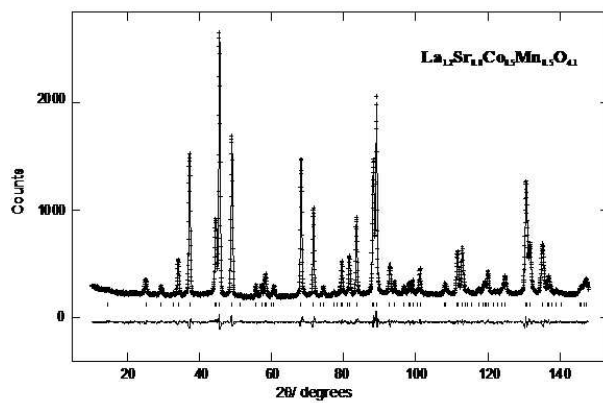


269x190mm (300 x 300 DPI)

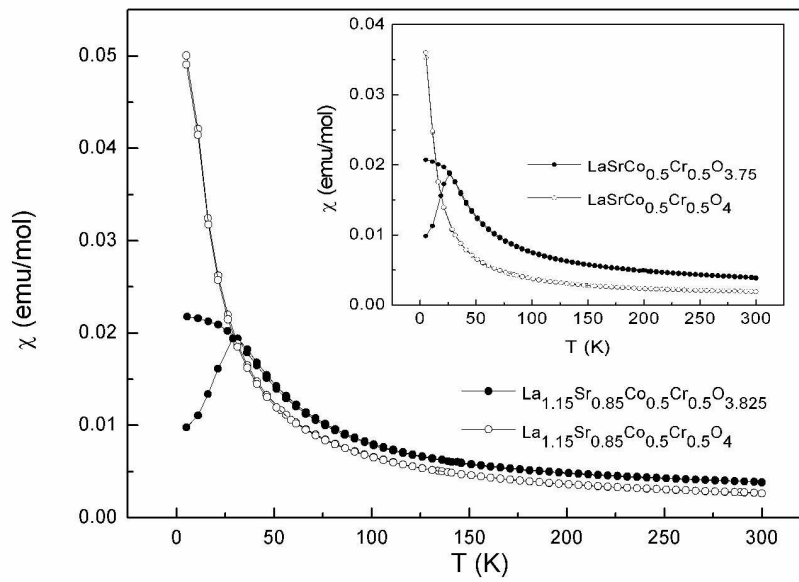
1
2
3
4
5
6
7
8
9
10
11
12
13
14
15
16
17
18
19
20
21
22
23
24
25
26
27
28
29
30
31
32
33
34
35
36
37
38
39
40
41
42
43
44
45
46
47
48
49
50
51
52
53
54
55
56
57
58
59
60



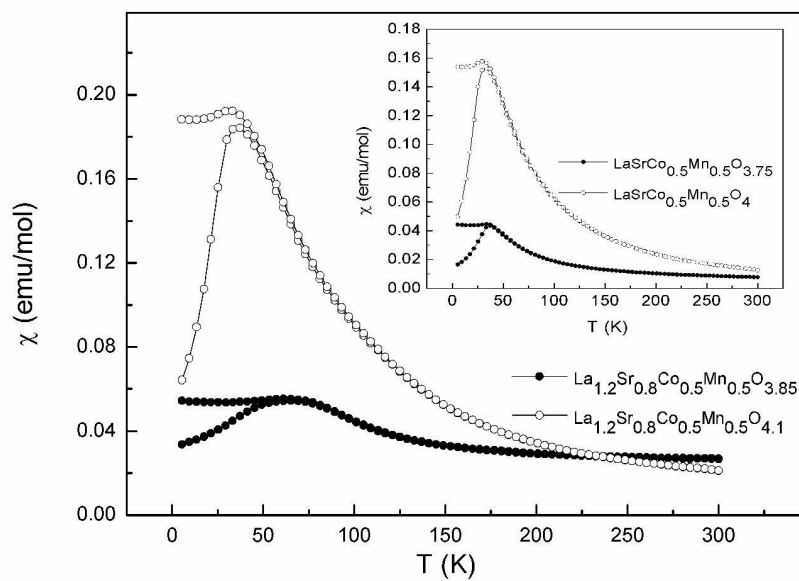
269x190mm (300 x 300 DPI)



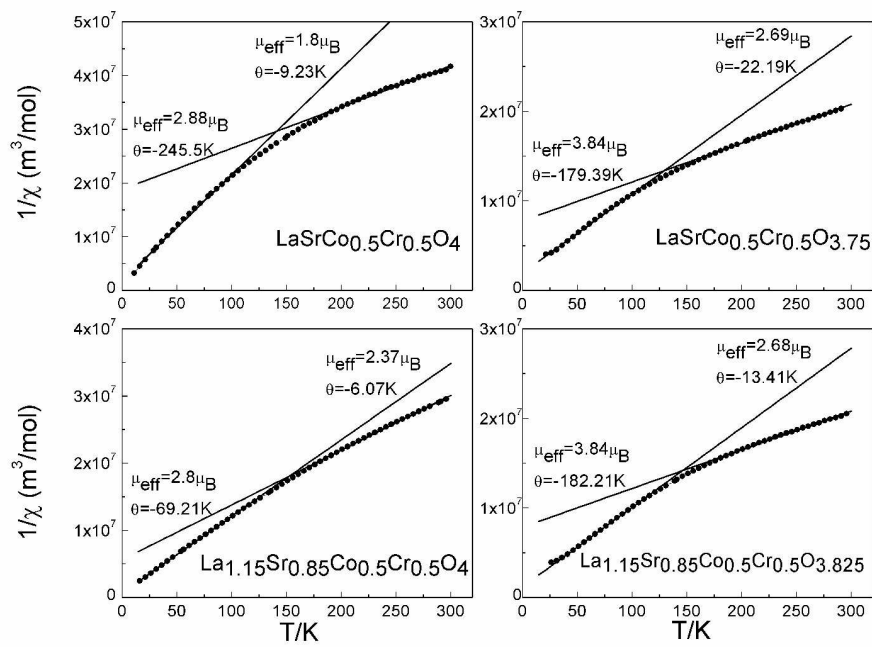
254x190mm (96 x 96 DPI)



269x190mm (300 x 300 DPI)

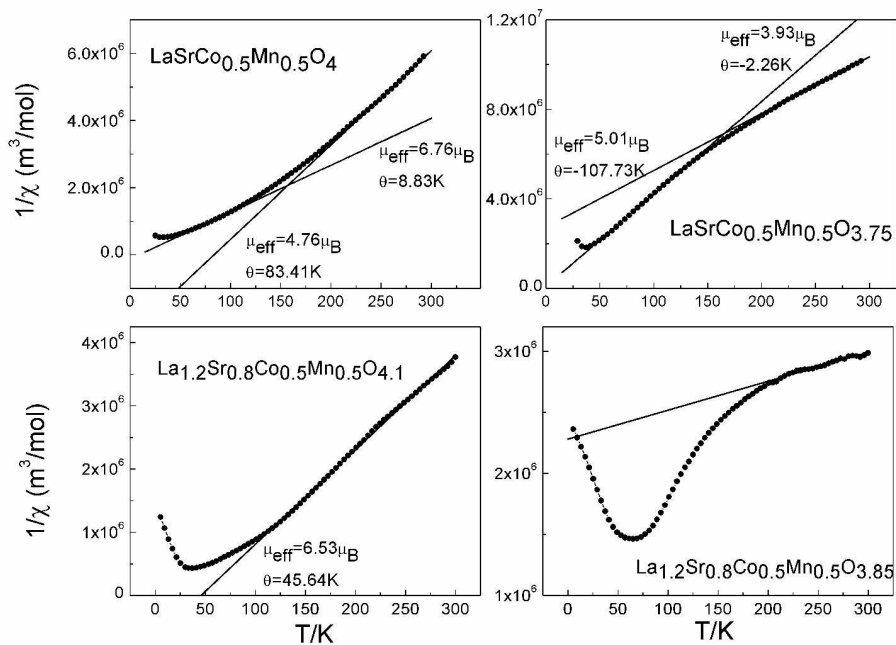


269x188mm (300 x 300 DPI)



269x206mm (300 x 300 DPI)

1
2
3
4
5
6
7
8
9
10
11
12
13
14
15
16
17
18
19
20
21
22
23
24
25
26
27
28
29
30
31
32
33
34
35
36
37
38
39
40
41
42
43
44
45
46
47
48
49
50
51
52
53
54
55
56
57
58
59
60



269x206mm (300 x 300 DPI)